Nanoscale

PAPER

View Article Online
View Journal | View Issue

Cite this: *Nanoscale*, 2019, **11**, 474

Diverse chiral assemblies of nanoparticles directed by achiral block copolymers *via* nanochannel confinement†

Qian Zhang, Jiabin Gu, Liangshun Zhang * and Jiaping Lin *

Received 30th August 2018,
Accepted 7th December 2018

DOI: 10.1039/c8nr07036a

rsc.li/nanoscale

It is a challenging task to realize large-area manufacture of chiral geometries of nanoparticles in solid-state materials, which exhibit strongly chiroptical responses in the visible and near-infrared ranges. Herein, novel nanocomposites, made from mixtures of achiral block copolymers and nanoparticles in a geometrically confined environment, are conceptually proposed to construct the chiral assemblies of nanoparticles through a joint theoretical-calculation framework and experimental discussion. It is found that the nanochannel-confined block copolymers self-assemble into a family of intrinsically chiral architectures, which serve as structural scaffolds to direct the chiral arrangement of nanoparticles. Through calculations of chiral order parameters and simulations of discrete dipole approximation, it is further demonstrated that certain members of this family of nanoparticle assemblies exhibit intense chiroptical activity, which can be tailored by the nanochannel radius and the nanoparticle loading. These findings highlight the multiple levels of structural control over a class of chiral assemblies of nanoparticles and the functionalities of emerging materials *via* careful design and selection of nanocomposites.

Introduction

Since the pioneering discovery of molecular chirality by Louis Pasteur,[1] optically active chiral materials have drawn a lot of attention due to their potential applications in the fields of biology and physics.[2–4] The chirality of natural molecules predominantly originates from the chiral configurations of sp^3-hybridized carbon atoms,[1] which gives rise to modest chiroptical responses in the ultraviolet spectral range and limits the practical versatility. Owing to the advent of engineering techniques at the nanoscale, it is possible to rationally and precisely create chiral assemblies comprising building blocks beyond the atomistic scale.[5] As promising candidates of optoelectronic materials, chiral assemblies of metal or semiconductor nanoparticles exhibit particularly high chiroptical activities in the visible and near-infrared ranges due to the high polarizability of materials.[6–8]

Currently, one of the most appealing proposals to yield the chiral assemblies is the directed self-assembly of pre-synthesized nanoparticles *via* chiral biomacromolecules such as DNA and peptides.[9–14] As typical examples, the DNA origami technique offers programmability in the geometry and metrics of the resultant nanoparticle assemblies.[15,16] However, the large-scale manufacture of nanoparticle assemblies requires a standard computerized synthesis of DNA molecules,[12,17] which still remains a hurdle for practical applications. Besides, the DNA origami technique is limited to the aqueous media and few kinds of nanoparticles compatible with DNA surface modification. Therefore, the large-area industrial manufacture of chiral assemblies of nanoparticles in device-friendly solid-state materials still remains a formidable challenge.

Driven by the balance between the incompatibility of various blocks and connectivity constraints of covalent bonds, block copolymers self-assemble into diverse periodically ordered structures at the nanometer scale.[18,19] These nanostructures can serve as structural scaffolds to host the spatial distribution of nanoparticles over a large area, which offer a viable route to fabricate the composite materials integrating the distinct properties of inorganic nanoparticles and organic polymers.[20,21] However, the self-assembled structures of block copolymers in bulk are always achiral and limited, and only a few studies have reported the chiral assemblies of nanoparticles in inorganic/organic composites.[22] A way to enrich the self-assembly behaviors of block copolymers is the utilization of geometrical confinement, which introduces frustration effects to break the symmetry of the self-assembled

Shanghai Key Laboratory of Advanced Polymeric Materials, State Key Laboratory of Bioreactor Engineering, Key Laboratory for Ultrafine Materials of Ministry of Education, School of Materials Science and Engineering, East China University of Science and Technology, Shanghai 200237, China. E-mail: zhangls@ecust.edu.cn, jlin@ecust.edu.cn

†Electronic supplementary information (ESI) available: Model and additional simulation results. See DOI: 10.1039/c8nr07036a

nanostructures.[23–25] In particular, the achiral block copolymers confined in nanochannels have the capability to produce intrinsically helical nanostructures.[26–33] Such fascinating nanostructures provide promising scaffolds to the direct assembly of nanoparticles into a helical arrangement. Nevertheless, the *a priori* prediction of chiral assemblies of nanoparticles from rationally designed nanocomposites still lacks a general roadmap and is yet to be demonstrated.

Motivated by the above issues, we herein report the first systematic investigation of novel nanocomposites, comprising the achiral block copolymer/nanoparticle mixtures in narrow nanochannels, for the construction of chiral assemblies of nanoparticles through the proposition of a joint theoretical–computational framework and experimental discussion (Fig. 1a). The advantage of the present study is that the intrinsically chiral nanostructures of achiral block copolymers, instead of the chiral biomacromolecules, offer well-defined scaffolds to build upon the chiral assemblies of nanoparticles with highly chiroptical activities. Specifically, through the mesoscopic hybrid particle-field model, it is definitely demonstrated that a vast collection of chiral assemblies of nanoparticles are readily accessible due to the symmetry breaking of the self-assembled nanostructures of achiral block copolymers in a confined environment. Furthermore, through the calculations of the chiral order parameter and discrete dipole approximation, it is found that the chirality of nanoparticle assemblies and their chiroptical responses are finely tuned by the modulation of the nanochannel radius and nanoparticle loading. Finally, the relationship between the existing experimental findings and our theoretical predictions is discussed, where we point out the wide implications of these results for rationally designing nanoparticle assemblies with desirable chiroptical activities in solid-state materials.

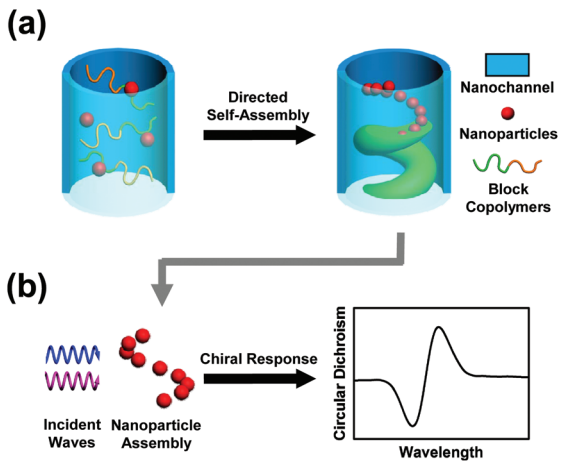

Fig. 1 (a) Schematic illustration of a hybrid particle-field model for the self-assembly of achiral block copolymer/nanoparticle composites confined in a nanochannel. (b) Schematic illustration of the simulations of circular dichroism spectra for the nanoparticle assemblies from the hybrid particle-field model. The spectra are calculated as the difference in extinction between the left- and right-handed circularly polarized incident waves as a function of wavelength.

Results and discussion

Nanoparticle assemblies directed by block copolymers

The hybrid particle-field (HPF) model is utilized to explore the self-assembled nanostructures of nanocomposites, which consist of achiral AB block copolymer chains and nanoparticles (designated as P).[34,35] A powerful feature of the HPF model is that the nanoparticle coordinates are explicitly retained as degrees of freedom. As illustrated in Fig. 1a, the nanocomposites are confined in a nanochannel with the radius R_W. The achiral block copolymers are modeled as the Gaussian chains with the gyration radius R_g. In our simulations, the block copolymers in the bulk self-assemble into hexagonally packed A-rich cylinders with a natural periodicity of $3.9R_g$, under the parameter settings of the A-block composition $f_A = 0.26$ and the combined Flory–Huggins interaction parameter $\chi_{AB}N = 20.0$. The walls (designated as W) of the nanochannels are neutral to the B blocks ($\chi_{BW}N = 0.0$) but repulsive to the A blocks ($\chi_{AW}N = 20.0$). For the cylinder-forming copolymers, the incorporation of nanochannels under various radii induces the entropy penalty of copolymer chains and thus encourages the formation of novel nanostructures (*i.e.*, single cylinder, stacked disks, single helix and double helix), which are illustrated in Fig. S1 of the ESI.† Interestingly, intrinsically chiral nanostructures, such as single and double helices, arise over a wide range of nanochannel radius (*i.e.*, $2.8R_g \leq R_W \leq 4.5R_g$).[26–32,36]

When the nanoparticles are incorporated into the confined block copolymers, the self-assembled nanostructures serve as scaffolds to direct the spatial distribution of nanoparticles. In our simulations, the effective radius of nanoparticles is chosen as $R_{P,e} = 0.4R_g$, including the contributions of the nanoparticle core and the grafted ligands. It is assumed that the nanoparticles are chemically identical to the A blocks (*i.e.*, $\chi_{AP}N = 0.0$ and $\chi_{BP}N = 20.0$), which can be experimentally realized by the surface functionalization of nanoparticles.[37–39] Fig. S2 of the ESI† displays the self-assembled nanostructures of nanocomposites with a lower loading of nanoparticles under various nanochannel radii R_W. The organization of nanoparticles closely resembles the self-assembled nanostructures of confined block copolymers, implying that the spatial distribution of nanoparticles can be programmed by the block copolymers. Meanwhile, the incorporation of nanoparticles impacts the conformation of polymer chains and contributes to the interparticle interactions. Therefore, varying the loading of nanoparticles could not only modulate the energetic contributions, but also tune the arrangement of nanoparticles.

Fig. 2a illustrates the effect of the nanoparticle loading c_P on the arrangement of nanoparticles directed by the confined block copolymers for the nanochannel radius $R_W = 2.6R_g$. Under these conditions, the achiral block copolymers self-assemble into A-rich single cylinders. In the top and side views, the distinct colors highlight the packing of nanoparticles in their assemblies. The three-dimensional view of the self-assembled nanostructures of nanocomposites is shown in Fig. S3a of the ESI.† At a lower loading of nano-

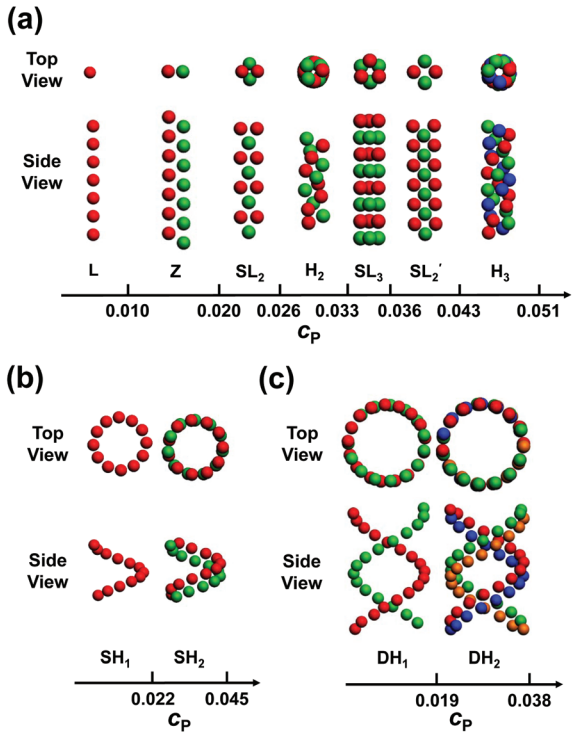

Fig. 2 Nanoparticle assemblies and the corresponding phase diagram in terms of the nanoparticle loading c_P for the nanochannel radius R_W = (a) $2.6R_g$, (b) $3.2R_g$ and (c) $4.1R_g$. In each panel, the top and side views illustrate the packing of nanoparticles at different layers or spirals, which are labeled by distinct colors for clarity. In panel (a), the nanoparticle assemblies are designated as L for the linear chain, Z for the zigzag arrangement, SL_n for the staggered layers with n nanoparticles, and H_n for the multi-stranded helix with n spirals. In panels (b) and (c), SH_n and DH_n stand for the n-layer single and double helices, respectively.

particles (c_P < 0.010), the nanoparticles are arranged into a linear chain (designated as L) at the center of the A-rich cylinder to relieve the entropic loss of the A blocks. With an increase of nanoparticle loading (0.010 < c_P < 0.020), a zigzag arrangement (Z) is achieved to maximize their filling fraction in the A-rich cylinder as well as alleviate the interparticle repulsions. However, upon increasing the nanoparticle loading, the interplay between nanoparticles becomes remarkable and the arrangement of nanoparticles deviates from the self-assembled nanostructures of confined block copolymers. As a consequence, the nanoparticles are guided to assemble into a rich library of assemblies including the staggered layers (SL_n) and multiple-stranded helices (H_n). In the range of 0.020 < c_P < 0.026, every two nanoparticles form staggered layers along the axis of the A-rich cylinder (SL_2). In the range of 0.026 < c_P < 0.033, the nanoparticles are guided to form double-stranded helices (H_2). Upon further increasing the nanoparticle loading, the nanoparticles form staggered layers consisting of three particles (SL_3), closely staggered layers consisting of two particles (SL'_2), and triple-stranded helices (H_3).[40–45]

In addition to the achiral nanostructures, the confined block copolymers have the capability to form intrinsically chiral nanostructures (*e.g.*, single and double helices), which serve as structural scaffolds to program the arrangement of nanoparticles. Fig. 2b and c show the nanoparticle assemblies directed by the confined block copolymers for the nanochannel radii $R_W = 3.2R_g$ and $4.1R_g$, respectively. The three-dimensional view of the self-assembled nanostructures of nanocomposites is shown in Fig. S3b and S3c of the ESI.† At a lower loading of nanoparticles, the nanoparticles are guided to form the one-layer single and double helices (SH_1 and DH_1) in the center of the A-rich domains due to weak interparticle interactions. With an increase of nanoparticle loading, such arrangements are unable to bear the increase of interparticle repulsions. To relieve the contribution from interparticle interactions, the nanoparticles are arranged into the double-layer helices (SH_2 and DH_2) along their axes. It should be mentioned that a higher loading of nanoparticles destroys the chiral nanostructures of confined block copolymers and triple-layer helices of nanoparticles are not observed in our simulations.

From Fig. 2, a universal rule underlying the various arrangements of nanoparticles can be captured, namely, the nanoparticle assemblies closely resemble the self-assembled nanostructures of the confined block copolymers under a low loading of nanoparticles, while an increase of nanoparticle loading results in complex arrangements. The assembly mechanisms of nanoparticles in the confined environment of block copolymers can be understood from the balances of enthalpy, entropy and frustration effects. On the one hand, the nanoparticles tend to maximize the filling fraction in the center of the A-rich domains for avoiding contact with the B-rich domains and minimize the deformation of the A blocks; on the other hand, the interparticle repulsions force them to distribute dispersedly in the A-rich domains. At a lower loading of nanoparticles, the arrangements of nanoparticle assemblies closely resemble the nanostructures of block copolymers due to their weak steric repulsions; thus, the self-assembled nanostructures of block copolymers serve as structural scaffolds to guide the formation of analogous assemblies for the nanoparticles. At a higher loading of nanoparticles, it is difficult to accommodate the nanoparticles in the center of the A-rich domains with a simple stacking way, because the interparticle interactions become important. As a consequence, the frustrated packing of nanoparticles (*i.e.*, the staggered layers, multi-stranded helices and multi-layer helices), which deviates from the self-assembled nanostructures of block copolymers, is achieved to alleviate the contribution of interparticle interactions.

It is worth pointing out that the nanoparticle size affects the self-assembled nanostructures of the nanocomposites. Fig. S4 of the ESI† illustrates the effect of the effective nanoparticle radius $R_{P,e}$ on the morphologies of the self-assembled structures of nanocomposites at various nanochannel radii $R_W = 2.6R_g$, $3.2R_g$ and $4.1R_g$. It is found that both the morphology of the self-assembled nanostructures and the arrangement of nanoparticles can be regulated by the variation of the effective nanoparticle radius, originating from the alleviation of the

conformational entropic penalty of polymer chains. The finding is generally in agreement with the theoretical and experimental observations.[46–48]

To characterize the chirality of nanoparticle assemblies, the chiral order parameter ξ is adopted to analyze the geometrical characteristics of nanoparticle assemblies directed by the confined block copolymers.[40] The chiral order parameter is defined as $\xi \equiv \left(\left|\Psi_{234}{}^2\right| + \left|\Psi_{346}{}^2\right| + \left|\Psi_{456}{}^2\right|\right)^{1/2}$, where $\Psi_{\mathrm{JKL}} = \sum_{mn} C(\mathrm{JKL}; mn)\rho_{\mathrm{J}m}\rho_{\mathrm{K}n}\rho^{*}_{\mathrm{L},m+n}$ denotes a series of pseudo-scalar parameters derived by Harris and co-workers.[49] Herein, C(JKL; mn) represents appropriate Clebsch–Gordan coefficients. $\rho_{\mathrm{J}m}$ is the multipole moment of the density field φ_{P} of nanoparticles through the spherical harmonics $Y_{\mathrm{J}m}$, namely, $\rho_{\mathrm{J}m} = \int \mathrm{d}\mathbf{r}\varphi_{\mathrm{P}}(\mathbf{r})Y_{\mathrm{J}m}$ and $\rho^{*}_{\mathrm{J}m} = (-1)^{m}\rho_{\mathrm{J},-m}$. A positive value of ξ implies that the nanoparticle assemblies are chiral, and the magnitude of ξ characterizes the strength of the chirality.

Fig. 3 presents the chiral order parameter ξ of the nanoparticle assemblies in terms of the nanoparticle loading c_{P} at the nanochannel radii $R_{\mathrm{W}} = 2.6R_g$, $3.2R_g$ and $4.1R_g$. There are two noteworthy features in the ξ–c_{P} plot. First of all, both nonzero and near-zero values of ξ are observed in the case of $R_{\mathrm{W}} = 2.6R_g$, where the confined block copolymers self-assemble into a single cylinder in the nanochannel. In particular, the nanoparticle assemblies in the regions of $0.026 < c_{\mathrm{P}} < 0.033$ and $0.043 < c_{\mathrm{P}} < 0.051$ have evidently nonzero values of the chiral order parameter, suggesting that the nanoparticles in the cylindrical domains of block copolymers are guided to form the chiral assemblies. Secondly, the chiral order parameters of nanoparticle assemblies for $R_{\mathrm{W}} = 3.2R_g$ and $4.1R_g$ are always larger than zero, because the structural scaffolds formed by the confined block copolymers have a feature of intrinsic chirality. More importantly, under these conditions, the values of the chiral order parameters are boosted as the nanoparticle loading increases. These phenomena manifest the fact that the chirality of nanoparticle assemblies is markedly enhanced by the chiral scaffolds of block copolymers confined in the nanochannels with a suitable radius. Meanwhile, the directed assembly of the confined block copolymers provides a higher degree of freedom to tailor the properties of nanoparticle assemblies, such as the collective chiroptical responses.

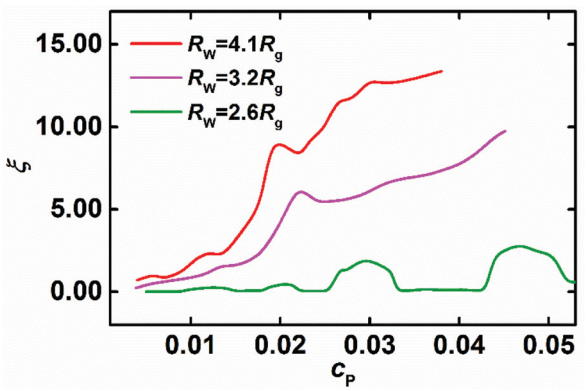

Fig. 3 Chiral order parameter ξ of nanoparticle assemblies as a function of the nanoparticle loading c_{P} under various nanochannel radii R_{W}. The definition of the chiral order parameter is presented in the main text.

Chiroptical responses of nanoparticle assemblies

The coordinates of nanoparticles in the HPF model are served as input configurations of discrete dipole approximation (DDA) simulations (Fig. 1b),[50] which are able to study the circular dichroism (CD) responses of plasmonic nanoparticle assemblies. In the DDA simulations, each nanoparticle is represented by an ensemble of dipoles such that the multipolar effects are accounted for. Herein, the nanoparticles are assumed to be gold (Au) nanoparticles with a radius of 4.0 nm (the gyration radius R_g of polymer chains is assumed to have a size of 10.0 nm). The real and imaginary parts of dielectric constants of Au nanoparticles are obtained from the literature of Johnson and Christy.[51] The background medium is assumed to be water, and the refractive index has a value of 1.333. We also calculate the CD spectra of nanoparticle assemblies embedded in the background of block copolymers (Fig. S5 of the ESI†). It is found that the CD spectra of nanoparticle assemblies embedded in different media exhibit a similar bisignated shape.

To ensure the high accuracy of CD spectra, the effects of the discretization degree and the replica number of nanoparticle assemblies on the numerical convergence of CD spectra are evaluated, which are shown in Fig. S6 and S7 of the ESI.† The CD spectra presented here are represented by the normalized intensity (*i.e.*, CD/N_{P}, where N_{P} is the number of nanoparticles in the simulated systems). Since the nanoparticle assemblies with near-zero values of the chiral order parameter ξ exhibit weak CD responses (Fig. S8 of the ESI†), we herein focus on the CD behavior of nanoparticle assemblies with larger values of ξ, including multiple-stranded helices (H_n), and single and double helices (SH_n and DH_n). Due to the lack of preferential handedness in the confined systems of nanocomposites, the right-handed assemblies of nanoparticles are considered as the input configurations of DDA simulations for calculating the CD spectra.

Fig. 4 shows the normalized CD spectra of double-stranded helices (H_2), one-layer single helices (SH_1), and one-layer double helices (DH_1). Herein, various loadings of nanoparticles are chosen to ensure the formation of defect-free assemblies. The calculated CD spectra of these assemblies exhibit bisignated dip-peak shape, implying the right-handed chiral arrangement of nanoparticle assemblies. Among these assemblies, the CD spectrum of the H_2 assembly exhibits relatively weak intensity and an asymmetric shape (inset of Fig. 4b). The weak CD responses of the H_2 assembly can be explained in terms of the degeneracy of the handedness. As illustrated in Fig. S9 of the ESI,† the H_n (n = 2 and 3) assemblies undergo both right- and left-handed twists depending on the choices of the helical baseline. The degeneracy of the

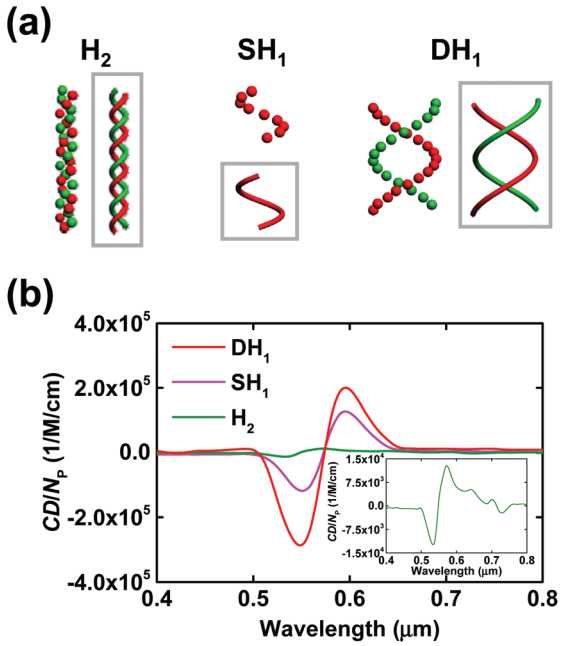

Fig. 4 (a) H_2, SH_1 and DH_1 assemblies of nanoparticles and their geometrical representation enclosed in the rectangles. (b) Simulated CD spectra of the H_2, SH_1 and DH_1 assemblies. The nanoparticles belonging to different spirals are labeled by distinct colors for clarity. The inset illustrates the CD spectrum of the H_2 assembly. The parameter settings of the nanochannel radius R_W and the nanoparticle loading c_P: (H_2) $R_W = 2.6R_g$ and $c_P = 0.029$; (SH_1) $R_W = 3.2R_g$ and $c_P = 0.019$; (DH_1) $R_W = 4.1R_g$ and $c_P = 0.019$.

right- and left-handed configurations weakens the preferential attenuation of circularly polarized lights, leading to the weak CD responses of the H_n assemblies. In comparison with the cases of the H_n assemblies, the SH_1 and DH_1 assemblies produce CD spectra with a symmetric dip-peak shape. In particular, the CD signals of the SH_1 and DH_1 assemblies have a magnitude of 10^5 $(M\ cm)^{-1}$, which is much larger than that of the nanoparticle helices prepared by the DNA origami technique.[10,52]

As illustrated above, the SH_n and DH_n assemblies of nanoparticles directed by the chiral scaffolds produce stronger and more stable CD signals. Meanwhile, the arrangement of nanoparticles is impacted by the nanoparticle loading c_P, which could affect the plasmonic interactions and the CD responses of nanoparticle assemblies. The CD spectra of the SH_n assemblies under various nanoparticle loadings c_P are calculated and presented in Fig. 5. Fig. 5a displays the representative CD spectra of the SH_n assemblies at various c_P under the nanochannel radius $R_W = 3.2R_g$. In the case of low nanoparticle loading (*i.e.*, $c_P = 0.013$), the amount of nanoparticles is insufficient to completely fill the center of the A-rich domain, and the nanoparticles organize into an SH_1 assembly with a large and non-uniform interparticle gap, as illustrated by the dashed spiral in Fig. 5a. Under this circumstance, the plasmonic interactions of nanoparticles are weak, which produces a CD signal with a small magnitude and asymmetric shape (inset of Fig. 5a). When the nanoparticle loading increases to $c_P = 0.022$, the nanoparticles in the SH_1 assembly become extremely close. This closely packed SH_1 assembly exhibits a CD signal with a characteristic dip-peak shape and intense intensity, suggesting the enhancement of plasmonic interactions in the assembly. As the nanoparticle loading further increases to $c_P = 0.045$, the arrangement of nanoparticles changes from SH_1 to SH_2. It is worth mentioning that the CD intensity of the SH_2 assembly is remarkably stronger than that of the SH_1 assembly. Moreover, the CD bands of the SH_2 assembly have red shifts, implying that the multipolar interactions play an important role in generating the CD signals of the SH_2 assembly. It should be pointed out that the nanoparticles are insufficient to form a defect-free SH_2 assembly in the range of $0.022 < c_P < 0.045$. However, as shown in Fig. S10 of the ESI,† the characteristic dip-peak shape of CD signals is stable against the defects, and the CD responses of the defective SH_2 assemblies remain strong.

To elucidate the effect of the nanoparticle loading c_P on the CD behaviors of the SH_n assemblies, the CD strength CD_{str} and the interparticle distance D_{avg}/D_P of the SH_n assemblies in terms of the nanoparticle loading c_P are plotted in Fig. 5b. The CD strength $CD_{str} = CD/N_P(peak) - CD/N_P(dip)$ is defined as the difference between the peak and dip values of the CD spectrum. As illustrated in Fig. 5a, D denotes the center-to-center distance between the neighboring nanoparticles and D_{avg} represents the average value. In the region of $c_P < 0.018$, the nanoparticles are separated by a long distance and the CD strengths of the nanoparticle assemblies are weak. With an increase of nanoparticle loading in this region, the CD strength displays a slight enhancement despite a drastic decrease of interparticle distance. As the nanoparticle loading exceeds 0.018, a different scenario is observed. The value of D_{avg}/D_P gradually approaches a constant value, but the magnitude of CD_{str} rapidly changes from 10^5 to 10^6 $(M\ cm)^{-1}$. The phenomena manifest the fact that the CD behaviors of nanoparticle assemblies are susceptible to the interparticle distance in the region of $c_P > 0.018$.

Fig. 5c plots the CD strength CD_{str} as a function of the interparticle distance D_{avg}/D_P for the SH_n assemblies. In the region of $D_{avg}/D_P > 1.5$, the multipolar interactions of nanoparticles are weak and the nanoparticles can be modelled as point dipoles in the CD calculations.[52] As a result, the variation of CD strength as a function of the interparticle distance obeys the power law $CD_{str} \propto (D_{avg}/D_P)^{-9.0}$. However, another power law of $CD_{str} \propto (D_{avg}/D_P)^{-9.8}$ is observed in the region of $D_{avg}/D_P < 1.5$. Such a change of the exponent of the power law indicates stronger multipolar interactions in the nanoparticle assemblies, which result in the intense CD signals with a magnitude of 10^6 $(M\ cm)^{-1}$. It should be mentioned that the exponential dependence of CD strength on the interparticle distance can be confirmed by other theoretical predictions. For instance, Fan *et al.* utilized the discrete dipole approximation to investigate the CD behaviors of the single helices of nanoparticles with various packing parameters η, which are determined by the interparticle distance D_{avg}.[53] A power law of $CD_{str} \propto \eta^{-9.67}$

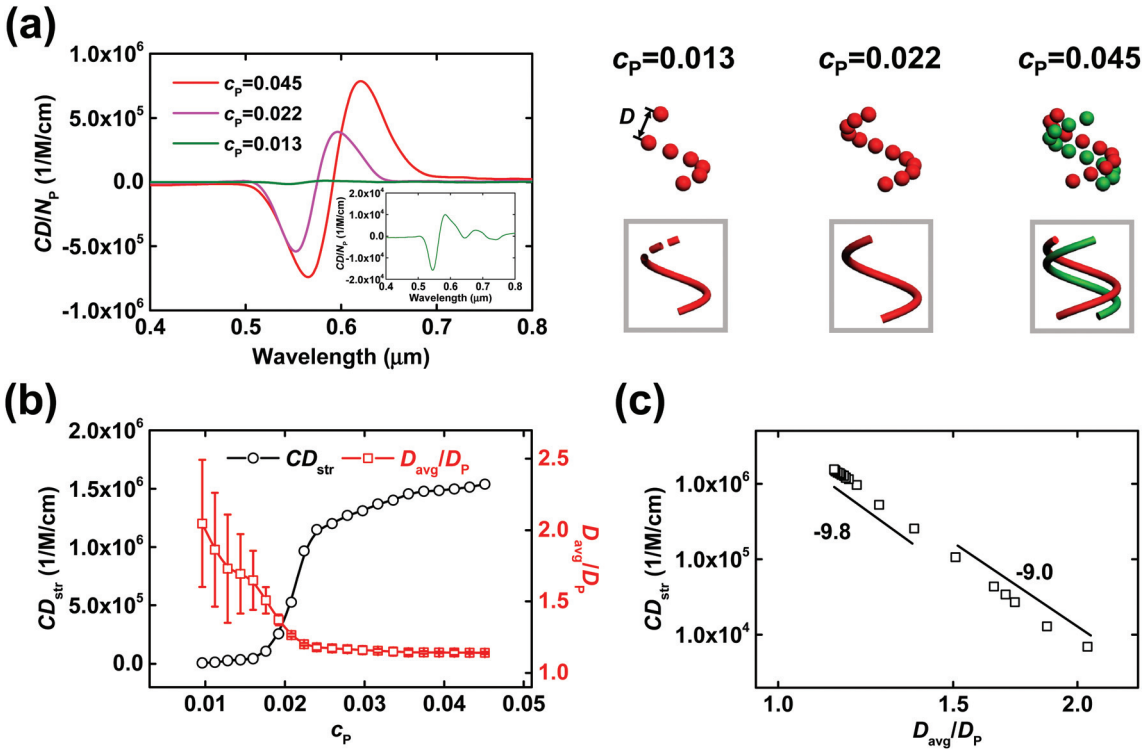

Fig. 5 (a) Simulated CD spectra of the SH_n assemblies at the nanochannel radius $R_W = 3.2R_g$ for various nanoparticle loadings c_P. The inset illustrates the CD spectrum for the case of $c_P = 0.013$. The right part shows the corresponding assemblies and their geometrical representations enclosed in the rectangles, where the dashed spiral indicates the defective arrangement of nanoparticles. (b) Variations of the CD strength CD_{str} and the interparticle distance D_{avg}/D_P as a function of the nanoparticle loading c_P. The CD strength $CD_{str} = CD/N_P(peak) - CD/N_P(dip)$ is defined as the difference between the peak and dip values in the CD spectra. D_{avg} denotes the averaged center-to-center distance of nanoparticles illustrated in panel (a), and D_P represents the diameter of nanoparticles. (c) The CD strength CD_{str} as a function of the interparticle distance D_{avg}/D_P. The plot is in logarithmic scale.

identified in their work is in good agreement with the relation $CD_{str} \propto (D_{avg}/D_P)^{-9.8}$ observed in our simulations. Therefore, the observations of Fig. 5 demonstrate the fact that the single helices of nanoparticles directed by the chiral scaffold have the characteristics of strong CD responses, which can be regulated by nanoparticle loading.

We further examine the CD behaviors of DH_n assemblies, which are depicted in Fig. 6. Similar to the case of SH_n assemblies, the DH_n assemblies of nanoparticles generate prominent CD signals, which have a tight relation with the nanoparticle loading in the nanocomposites (Fig. 6a). As further demonstrated in Fig. 6b, an increase of the nanoparticle loading c_P also leads to a decrease of the interparticle distance D_{avg}/D_P and an increase of the CD strength CD_{str}. The variation of CD_{str} as a function of D_{avg}/D_P can be also divided into two regimes: the power law of $CD_{str} \propto (D_{avg}/D_P)^{-7.1}$ exists in the region of $D_{avg}/D_P > 1.5$ and $CD_{str} \propto (D_{avg}/D_P)^{-7.9}$ is observed in the region of $D_{avg}/D_P < 1.5$ (Fig. 6c). However, in comparison with the case of the SH_n assemblies, the exponents of the power law in the case of the DH_n assemblies have smaller absolute values.

The discrepancy between the CD behaviors of the SH_n and DH_n assemblies may be attributed to two factors: the intra- and inter-helix interactions of nanoparticles. On the one hand, the SH_n and DH_n assemblies have different pitch lengths, which impact the intra-helix plasmonic interactions of nanoparticles in these assemblies. On the other hand, the CD responses of the DH_n assemblies are also influenced by the inter-helix plasmonic coupling between the isolated strands. To pinpoint the principal factor of nanoparticle interactions on the CD behaviors, we calculate the CD spectra of isolated strands decomposed from the DH_n assemblies. As illustrated in Fig. S11 of the ESI,† the CD spectra of isolated strands are very close to that of the DH_n assembly, indicating that the inter-helix interactions in the DH_n assemblies are negligible. Therefore, the discrepancy between the CD behaviors of the SH_n and DH_n assemblies originates from the difference in the intra-helix interactions. In other words, the pitch length of the nanoparticle helix affects its CD responses, which are demonstrated by the experimental observation.[54] In our simulations, the pitches of the DH_n assemblies are larger than those of the SH_n assemblies, which stems from the intrinsic feature of the structural scaffold of confined block copolymers. For instance, the SH_1 and DH_1 assemblies have pitches of ~40 nm and ~80 nm at the nanoparticle loading $c_P = 0.019$, respectively. This difference results in the smaller absolute value of the

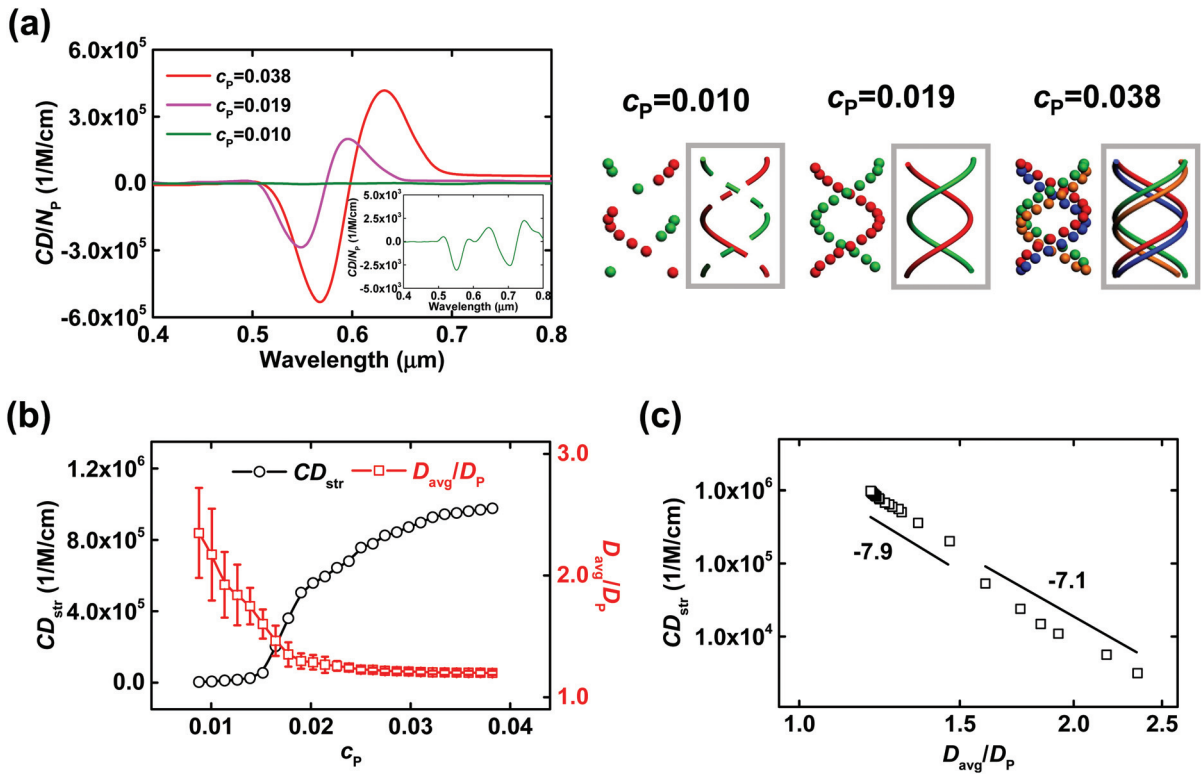

Fig. 6 (a) Simulated CD spectra of the DH_n assemblies at the nanochannel radius $R_W = 4.1R_g$ for various nanoparticle loadings c_P. The inset illustrates the CD spectrum for the case of $c_P = 0.010$. The right part shows the corresponding assemblies and their geometrical representations enclosed in the rectangles. (b) Variations of the CD strength CD_{str} and the interparticle distance D_{avg}/D_P as a function of the nanoparticle loading c_P. (c) The CD strength CD_{str} as a function of the interparticle distance D_{avg}/D_P. The plot is in logarithmic scale.

exponents in the power laws of the DH_n assemblies (Fig. 6c), implying that an increase of pitch length weakens the multipolar interactions of nanoparticles in the helices. This relation between the structural characteristics and the CD properties provides a guideline for rationally designing the chiral assemblies of nanoparticles and their chiroptical activities.

In addition to the CD spectra, the chiroptical activity of chiral assemblies can also be evaluated by the anisotropic dissymmetry factor (*g*-factor). The *g*-factor is defined as the ratio of circular dichroism to extinction, *i.e.*, $g = 2(Q_{ext,+} - Q_{ext,-})/(Q_{ext,+} + Q_{ext,-})$, where $Q_{ext,+}$ and $Q_{ext,-}$ are, respectively, the extinction efficiency factors for the left- and right-handed circularly polarized light.[55] As shown in Fig. 7a, the *g*-factor spectra of the SH_1 and DH_1 assemblies display bisignated dip-peak shapes, which are similar to their CD spectra. Furthermore, the maximum absolute value ($|g|_{max}$) of the anisotropic dissymmetry factor is introduced to compare our predicted results with the experimental observations. Fig. 7b shows the maximum value ($|g|_{max}$) for the single and double helices of nanoparticles as a function of the nanoparticle loading c_P. The maximum value of the *g*-factor is significantly boosted by an increase of the nanoparticle loading c_P. In particular, the maximum values $|g|_{max}$ of the *g*-factor for the single and double helices of nanoparticles can, respectively, reach values of 0.09 and 0.07, which are higher than the typical values for the naturally chiral materials (in the range of $\sim10^{-7}$ to $\sim10^{-5}$) and for most of the DNA-guided chiral assemblies (in the range of $\sim10^{-3}$ to $\sim10^{-2}$).[10,56,57] These results definitely demonstrate that the CD signals of the chiral assemblies of nanoparticles are much stronger than those of the chiral molecules and nanoparticle assemblies prepared by the DNA origami technique.

It is instructive to assess the influence of the physiochemical properties of nanoparticles on their assemblies and the chiroptical activities, which are illustrated in Fig. S12 and S13 of the ESI.† It is found that the assemblies of the smaller nanoparticles have a weaker CD strength and blue shifts of CD bands, which are consistent with the previous experimental observations.[10] In addition, when the interparticle interactions are enhanced, the nanoparticles in the environment of geometric confinement are unable to form closely packed assemblies, which are not ideal candidates for creating functional materials with highly chiroptical activities.

Experimental discussion

To the best of our knowledge, there are no direct experimental studies on the chiral assemblies of nanoparticles programmed by the chiral scaffolds of achiral block copolymers and their

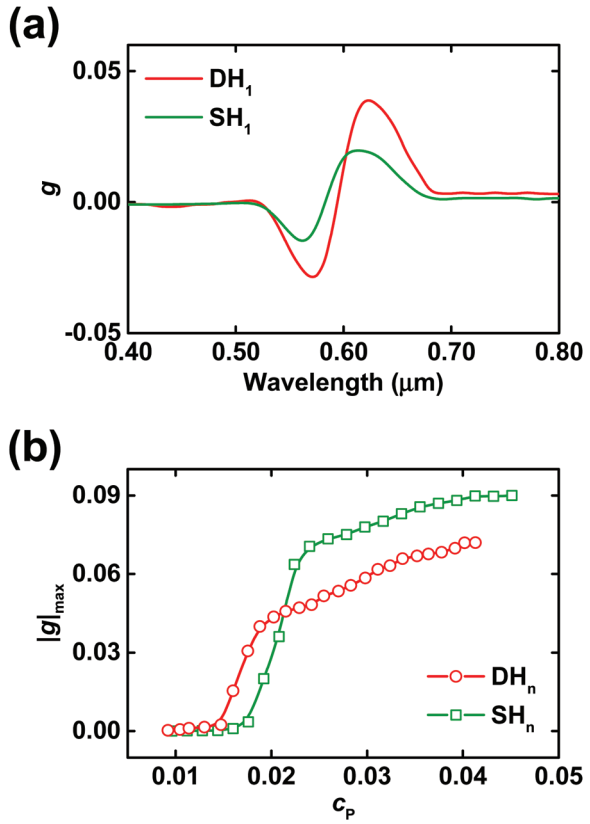

Fig. 7 (a) Anisotropic dissymmetry factor (g-factor) of the SH_1 and DH_1 assemblies as a function of the wavelength. The nanoparticle loadings of the SH_1 and DH_1 assemblies are set as $c_P = 0.019$. (b) Maximum absolute value ($|g|_{max}$) of the anisotropic dissymmetry factor of the SH_n and DH_n assemblies as a function of the nanoparticle loading c_P. The nanochannel radii for the SH_n and DH_n assemblies are set as $R_W = 3.2R_g$ and $4.1R_g$, respectively.

CD responses. Therefore, it is difficult to make direct comparisons between the experimental observations and the theoretical predictions. However, there still exist some experimental findings regarding the nanoparticle assemblies of polymer/nanoparticle composites *via* nanochannel confinement, which support our results of self-assembled nanostructures and their CD responses.[58,59] For instance, upon imposing cylindrical confinement onto the block copolymer/small molecule/nanoparticle blends, Xu and co-authors prepared a variety of nanoparticle assemblies (including isolated dot, one-dimensional line, single- and double-stranded helices) in the cylinders of block copolymers, which are tuned by the loading of nanoparticles (Fig. 4 in ref. 55). Furthermore, it is demonstrated that the assemblies of nanoparticles possess a chiroptical response at the near-infrared region. In our simulations of the hybrid particle-field model, the block copolymer/nanoparticle composites confined in the narrower nanochannels self-assemble into a much richer variety of nanoparticle assemblies including the linear chain and helices (Fig. 2a), which can be tailored by the nanoparticle loading. In addition, the calculations of the chiral order parameter and CD spectra clearly demonstrate that several nanoparticle assemblies have the characteristics of chirality and chiroptical activity (case of $R_W = 2.6R_g$ in Fig. 3 and 4). Despite the use of simple block copolymers and the structural diversity observed in our simulations, the good agreement between the experimental observations and the theoretical predictions unequivocally confirms the role of self-assembled nanostructures of confined block copolymers for the arrangement of nanoparticles.

More importantly, beyond reproducing the nanoparticle assemblies observed in the experimental work,[58] we also predict a variety of novel chiral structures of nanoparticle ensembles *via* changing the radius of nanochannels (Fig. 2b and c). The intrinsically chiral nanostructures of confined block copolymers for the first time, to the best of our knowledge, serve as structural scaffolds to direct the sophisticated assembly of nanoparticles into the chiral arrangement (*i.e.*, SH_n and DH_n assemblies in Fig. 2). The CD signals of the SH_n and DH_n assemblies have a magnitude of 10^5 $(M\ cm)^{-1}$, which is much larger than that of the multi-stranded helices H_n (Fig. 4). Furthermore, the CD responses of nanoparticle assemblies can be noticeably enhanced by increasing the nanoparticle loading (Fig. 5 and 6). From the experimental perspective, the self-assembly of the achiral block copolymers confined in the nanochannels provides a practical solution to the fabrication of the structural scaffolds with an intrinsically chiral feature over a large area, owing to the existence of a variety of approaches for the geometric confinement (such as the anodized aluminum oxide (AAO) membrane and the polydimethylsiloxane porous membrane).[25,60] For instance, Dobriyal *et al.* prepared a series of AAO membranes with the pore radius R_W ranging from 20 to 40 nm, which serve as the confined environment of nanochannels to direct the self-assembly of polystyrene-*b*-polybutadiene copolymers with the gyration radius in the range of $10 \leq R_g \leq 20$ nm.[30] The experimental observations of single and double helices confirm that the nanochannels adopted in our simulations are currently available in the experiments. Therefore, the strategy of chiral nanostructures of a confined block of copolymers opens the opportunity to access and manipulate the chiral arrangements of nanoparticles, which give rise to the prominent and characteristic CD signals in the range of visible light. Looking ahead to possible applications, these assemblies of nanoparticles with chiral arrangement and strong CD responses offer potential in the fields of biosensing, optoelectronics and negative refractive index materials.[2–4]

In experiments, functionalizing the nanoparticles with a variety of ligand chains such as oligomeric surfactants and grafted homopolymers has emerged as a popular approach to stabilize and distribute the nanoparticles in polymer matrices.[37–39] The physicochemical properties of ligand chains can be incorporated into the hybrid particle-field (HPF) model *via* the particle–polymer interface, which plays a critical role in the self-assembly of block copolymer-based nanocomposites. To demonstrate the validity of such treatment in the HPF model, we use the self-consistent field theory to describe the system of ligand-grafted nanoparticles immersed in a homopolymer matrix,[61] as illustrated in Fig. S14 of the ESI.† It is

confirmed that the layer of grafting ligands can be simplified as the nanoparticle–polymer interfacial region surrounding the nanoparticle. The width of the particle–polymer interface is impacted by the grafting density, the grafting ligand–homopolymer interaction parameter and the length ratio of homopolymers to ligands. The calculation results are generally consistent with the theoretical predictions and experimental observations of Composto and co-workers.[62,63]

Finally, we would like to point out that the left- and right-handed helices of nanoparticles have equal probability, which is the nature of the spontaneous symmetry breaking of the self-assembled nanostructures for the confined system. There also exist some investigations to manipulate the handedness of the self-assembled nanostructures of the achiral block copolymers confined in nanochannels.[64,65] For instance, Deng *et al.* designed a chiral pattern onto the inner surface of nanochannels to direct the self-assembly of block copolymers.[64] It is illustrated that the helical chirality of the self-assembled nanostructures of the achiral block copolymers can be delicately controlled by the tailored surface patterns. It is possible to extend the strategy of predefined surface patterns to determine the handedness of the self-assembled nanostructures of block copolymer/nanoparticle composites, and to investigate the CD responses of nanoparticle assemblies with the prescribed handedness.

Conclusions

Through the proposal of a joint theoretical–computational framework and an experimental discussion, we present the first systematic investigation of the chirality and the circular dichroism responses of nanoparticle assemblies programmed by the intrinsically chiral nanostructures of nanochannel-confined block copolymers. The good agreement between the experimental observations and the theoretical predictions yields a fundamental insight into the mechanisms on how the block copolymers are exploited to direct the chiral assemblies of nanoparticles. Furthermore, our study demonstrates that a rich variety of nanoparticle assemblies, which cannot be currently obtained in the experimental studies, are achieved by finely tuning the nanochannel radius and the nanoparticle loading. Through an evaluation of the chiral order parameter and circular dichroism responses, it is clearly demonstrated that the chirality of nanoparticle assemblies is markedly improved by the intrinsically chiral scaffolds of the self-assembled nanostructures of the confined block copolymers. These findings suggest a new insight into the physical mechanism of experimental observations and may possess wide implications in the fabrication of emerging materials with multiple functionalities.

Computational model

Hybrid particle-field model

The hybrid particle-field (HPF) model in the three-dimensional space is used to explore the self-assembly of the achiral AB block copolymer/nanoparticle (designated as P) composites confined in the nanochannel (W) with the radius R_W. The system consists of n monodisperse AB copolymers and n_P nanoparticles. The achiral block copolymers are modeled as the Gaussian chains in the field-theoretical framework of inhomogeneous polymeric fluids. The polymer chains have a gyration radius of $R_g = b(N/6)^{1/2}$, where N is the segment number of a single chain and b is the statistical segment length. The composition of A blocks in the polymer chains is denoted by f_A. The nanoparticles with the effective radius $R_{P,e}$ are represented by a cavity function. The coordinates of nanoparticles are explicitly retained as degrees of freedom. The nanoparticle loading in the composites is denoted by c_P. The polymer chains are excluded from the inside of nanoparticles upon the enforcement of a local incompressibility constraint. Interactions between the distinct components are described by the combined Flory–Huggins parameters $\chi_{IJ}N$ (I, J = A, B, P and W). More details on the theoretical model and parameter settings for the nanocomposites are presented in Part IX of the ESI.†

Simulations of circular dichroism spectra

To calculate the circular dichroism (CD) spectra of nanoparticle assemblies, the coordinates of nanoparticles in the HPF model are served as input parameters of the DDSCAT 7.3 package developed by Draine and Flatau,[50] which is able to study the absorption, scattering and near-fields of plasmonic nanostructures with varied properties through the discrete dipole approximation (DDA).[66–68] In the DDA approach, each individual nanoparticle is represented by an ensemble of identical dipoles such that the multipolar effects are accounted for. In the presence of an incident wave, the fields experienced by a single dipole consist of the incident fields and the fields induced by other dipoles. Therefore, the dipole polarizations can be achieved by solving a set of coupled linear equations. By iteratively solving the dipole polarizations, the extinction cross sections of nanoparticle assemblies for left-handed circularly polarized (LCP) and right-handed circularly polarized (RCP) incident waves can be derived. The CD spectrum is obtained from averaging the difference of extinction cross sections between the LCP and RCP incident waves for many orientations of incident waves. More details regarding the CD calculations are presented in Part X of the ESI.†

Conflicts of interest

There are no conflicts to declare.

Acknowledgements

This work was supported by the National Natural Science Foundation of China (21574040, 21873029 and 51833003).

Notes and references

1 L. Pasteur, *Ann. Chim. Phys. Sér.*, 1848, **3**, 442–459.
2 R. Quidant and M. Kreuzer, *Nat. Nanotechnol.*, 2010, **5**, 762–763.
3 J. B. Pendry, *Science*, 2004, **306**, 1353–1355.
4 J. K. Gansel, M. Thiel, M. S. Rill, M. Decker, K. Bade, V. Saile, G. von Freymann, S. Linden and M. Wegener, *Science*, 2009, **325**, 1513–1515.
5 M. Yang and N. A. Kotov, *J. Mater. Chem.*, 2011, **21**, 6775–6792.
6 X. Peng, N. Komatsu, S. Bhattacharya, T. Shimawaki, S. Aonuma, T. Kimura and A. Osuka, *Nat. Nanotechnol.*, 2007, **2**, 361–365.
7 J. Yeom, B. Yeom, H. Chan, K. W. Smith, S. Dominguez-Medina, J. H. Bahng, G. Zhao, W.-S. Chang, S.-J. Chang, A. Chuvilin, D. Melnikau, A. L. Rogach, P. Zhang, S. Link, P. Král and N. A. Kotov, *Nat. Mater.*, 2015, **14**, 66–72.
8 W. Ma, L. Xu, A. F. de Moura, X. Wu, H. Kuang, C. Xu and N. A. Kotov, *Chem. Rev.*, 2017, **117**, 8041–8093.
9 X. Shen, C. Song, J. Wang, D. Shi, Z. Wang, N. Liu and B. Ding, *J. Am. Chem. Soc.*, 2012, **134**, 146–149.
10 A. Kuzyk, R. Schreiber, Z. Fan, G. Pardatscher, E.-M. Roller, A. Högele, F. C. Simmel, A. O. Govorov and T. Liedl, *Nature*, 2012, **483**, 311–314.
11 A. Kuzyk, R. Schreiber, H. Zhang, A. O. Govorov, T. Liedl and N. Liu, *Nat. Mater.*, 2014, **13**, 862–866.
12 S. J. Tan, M. J. Campolongo, D. Luo and W. Cheng, *Nat. Nanotechnol.*, 2011, **6**, 268–276.
13 H.-E. Lee, H.-Y. Ahn, J. Mun, Y. Y. Lee, M. Kim, N. H. Cho, K. Chang, W. S. Kim, J. Rho and K. T. Nam, *Nature*, 2018, **556**, 360–365.
14 C. Zhou, X. Duan and N. Liu, *Acc. Chem. Res.*, 2017, **50**, 2906–2914.
15 W. Chen, A. Bian, A. Agarwal, L. Liu, H. Shen, L. Wang, C. Xu and N. A. Kotov, *Nano Lett.*, 2009, **9**, 2153–2159.
16 Y. Tian, T. Wang, W. Liu, H. L. Xin, H. Li, Y. Ke, W. M. Shih and O. Gang, *Nat. Nanotechnol.*, 2015, **10**, 637–644.
17 A. M. Hung, C. M. Micheel, L. D. Bozano, L. W. Osterbur, G. M. Wallraff and J. N. Cha, *Nat. Nanotechnol.*, 2009, **5**, 121–126.
18 M. Park, C. Harrison, P. M. Chaikin, R. A. Register and D. H. Adamson, *Science*, 1997, **276**, 1401–1404.
19 W. Li and M. Müller, *Prog. Polym. Sci.*, 2016, **54**, 47–75.
20 L.-T. Yan and X.-M. Xie, *Prog. Polym. Sci.*, 2013, **38**, 369–405.
21 A. C. Balazs, T. Emrick and T. R. Russell, *Science*, 2006, **314**, 1107–1110.
22 Z. Li, K. Hur, H. Sai, T. Higuchi, A. Takahara, H. Jinnai, S. M. Gruner and U. Wiesner, *Nat. Commun.*, 2014, **5**, 3247.
23 K. Shin, H. Q. Xiang, S. I. Moon, T. Kim, T. J. McCarthy and T. P. Russell, *Science*, 2004, **306**, 76–76.
24 H. Wu, Y. Higaki and A. Takahara, *Prog. Polym. Sci.*, 2018, **77**, 95–117.
25 C. Mijangos, R. Hernandez and J. Martin, *Prog. Polym. Sci.*, 2016, **54**, 148–182.
26 Y. Wu, G. Cheng, K. Katsov, S. W. Sides, J. Wang, J. Tang, G. H. Fredrickson, M. Moskovits and G. D. Stucky, *Nat. Mater.*, 2004, **3**, 816–822.
27 B. H. Jones and T. P. Lodge, *ACS Nano*, 2011, **5**, 8914–8927.
28 H. Kim, S. Lee, T. J. Shin, E. Korblova, D. M. Walba, N. A. Clark, S. B. Lee and D. K. Yoon, *Proc. Natl. Acad. Sci. U. S. A.*, 2014, **111**, 14342–14347.
29 H. Xiang, K. Shin, T. Kim, S. I. Moon, T. J. McCarthy and T. P. Russell, *Macromolecules*, 2005, **38**, 1055–1056.
30 P. Dobriyal, H. Xiang, M. Kazuyuki, J.-T. Chen, H. Jinnai and T. P. Russell, *Macromolecules*, 2009, **42**, 9082–9088.
31 B. Yu, P. Sun, T. Chen, Q. Jin, D. Ding, B. Li and A.-C. Shi, *Phys. Rev. Lett.*, 2006, **96**, 138306.
32 D. Chen, S. Park, J.-T. Chen, E. Redston and T. P. Russell, *ACS Nano*, 2009, **3**, 2827–2833.
33 V. Kalra, J. H. Lee, J. H. Park, M. Marquez and Y. L. Joo, *Small*, 2009, **5**, 2323–2332.
34 S. W. Sides, B. J. Kim, E. J. Kramer and G. H. Fredrickson, *Phys. Rev. Lett.*, 2006, **96**, 250601.
35 Q. Zhang, L. Zhang and J. Lin, *J. Phys. Chem. C*, 2017, **121**, 23705–23715.
36 W. Li and R. A. Wickham, *Macromolecules*, 2006, **39**, 8492–8498.
37 R. Mout, D. F. Moyano, S. Rana and V. M. Rotello, *Chem. Soc. Rev.*, 2012, **41**, 2539–2544.
38 C. Yi, S. Zhang, K. T. Webb and Z. Nie, *Acc. Chem. Res.*, 2017, **50**, 12–21.
39 J. J. Chiu, B. J. Kim, E. J. Kramer and D. J. Pine, *J. Am. Chem. Soc.*, 2005, **127**, 5036–5037.
40 G. T. Pickett, M. Gross and H. Okuyama, *Phys. Rev. Lett.*, 2000, **85**, 3652–3655.
41 H.-K. Chan, *Phys. Rev. E: Stat., Nonlinear, Soft Matter Phys.*, 2011, **84**, 050302.
42 A. Mughal, H. K. Chan and D. Weaire, *Phys. Rev. Lett.*, 2011, **106**, 115704.
43 A. Mughal, H. K. Chan, D. Weaire and S. Hutzler, *Phys. Rev. E: Stat., Nonlinear, Soft Matter Phys.*, 2012, **85**, 051305.
44 G. Wu, H. Cho, D. A. Wood, A. D. Dinsmore and S. Yang, *J. Am. Chem. Soc.*, 2017, **139**, 5095–5101.
45 S. Sanwaria, A. Horechyy, D. Wolf, C.-Y. Chu, H.-L. Chen, P. Formanek, M. Stamm, R. Srivastava and B. Nandan, *Angew. Chem., Int. Ed.*, 2014, **53**, 9090–9093.
46 R. B. Thompson, V. V. Ginzburg, M. W. Matsen and A. C. Balazs, *Science*, 2001, **292**, 2469–2472.
47 M. R. Bockstaller and E. L. Thomas, *Phys. Rev. Lett.*, 2004, **93**, 166106.
48 M. R. Bockstaller, Y. Lapetnikov, S. Margel and E. L. Thomas, *J. Am. Chem. Soc.*, 2003, **125**, 5276–5277.
49 A. B. Harris, R. D. Kamien and T. C. Lubensky, *Rev. Mod. Phys.*, 1999, **71**, 1745–1757.
50 P. J. Flatau and B. T. Draine, *Opt. Express*, 2012, **20**, 1247–1252.
51 P. B. Johnson and R. W. Christy, *Phys. Rev. B: Solid State*, 1972, **6**, 4370–4379.
52 Z. Fan and A. O. Govorov, *Nano Lett.*, 2010, **10**, 2580–2587.
53 Z. Fan, H. Zhang and A. O. Govorov, *J. Phys. Chem. C*, 2013, **117**, 14770–14777.

54 S. Mokashi-Punekar, A. D. Merg and N. L. Rosi, *J. Am. Chem. Soc.*, 2017, **139**, 15043–15048.
55 N. Berova, L. D. Bari and G. Pescitelli, *Chem. Soc. Rev.*, 2007, **36**, 914–931.
56 W. Ma, H. Kuang, L. G. Xu, L. Ding, C. L. Xu, L. B. Wang and N. A. Kotov, *Nat. Commun.*, 2013, **4**, 2689.
57 L. D. Barron, *Molecular light scattering and optical activity*, Cambridge University Press, 2004.
58 P. Bai, S. Yang, W. Bao, J. Kao, K. Thorkelsson, M. Salmeron, X. Zhang and T. Xu, *Nano Lett.*, 2017, **17**, 6847–6854.
59 R. Liang, J. Xu, R. Deng, K. Wang, S. Liu, J. Li and J. Zhu, *ACS Macro Lett.*, 2014, **3**, 486–490.
60 B. Pokroy, A. K. Epstein, M. C. M. Persson-Gulda and J. Aizenberg, *Adv. Mater.*, 2009, **21**, 463–469.
61 T. L. Chantawansri, S.-M. Hur, C. J. García-Cervera, H. D. Ceniceros and G. H. Fredrickson, *J. Chem. Phys.*, 2011, **134**, 244905.
62 A. L. Frischknecht, M. J. A. Hore, J. Ford and R. J. Composto, *Macromolecules*, 2013, **46**, 2856–2869.
63 J. Choi, M. J. A. Hore, J. S. Meth, N. Clarke, K. I. Winey and R. J. Composto, *ACS Macro Lett.*, 2013, **2**, 485–490.
64 H. Deng, Y. Qiang, T. Zhang, W. Li and T. Yang, *Nanoscale*, 2016, **8**, 15961–15969.
65 H. K. Choi, J.-B. Chang, A. F. Hannon, J. K. W. Yang, K. K. Berggren, A. Alexander-Katz and C. A. Ross, *Nano Futures*, 2017, **1**, 015001.
66 C. Song, M. G. Blaber, G. Zhao, P. Zhang, H. C. Fry, G. C. Schatz and N. L. Rosi, *Nano Lett.*, 2013, **13**, 3256–3261.
67 R. Guo, J. Mao, X.-M. Xie and L.-T. Yan, *Sci. Rep.*, 2014, **4**, 7021.
68 Y. Xie, L. Carbone, C. Nobile, V. Grillo, S. D'Agostino, F. D. Sala, C. Giannini, D. Altamura, C. Oelsner, C. Kryschi and P. D. Cozzoli, *ACS Nano*, 2013, **7**, 7352–7369.